Effects of Soil Physical Nonuniformity on Chamber-Based Gas Flux Estimates

Rodney T. Venterea*
John M. Baker
USDA-ARS
Soil and Water Research Management Unit
439 Borlaug Hall
1991 Upper Buford Cir.
St. Paul, MN 55108

Chamber methods for measuring trace gas fluxes are prone to errors resulting in large part from the alteration of near-surface concentration gradients. There is little information available, however, for quantifying these errors or determining how they vary with soil physical properties, chamber deployment methods, and flux calculation schemes. This study used numerical modeling to examine how these factors influence flux estimate errors in physically uniform and nonuniform soil profiles. Errors varied widely among profiles and flux calculation techniques. Soil profiles having identical predeployment fluxes but differing in water content and bulk density generated substantially different flux chamber data. A theoretical flux model that assumes physical uniformity performed relatively well in nonuniform soils but still generated substantial errors. For all flux models, errors were minimized with larger effective chamber heights (h) and shorter deployment times (DT). In light of these findings, recent studies that recommend minimizing h and extending DT to enhance nonlinearity of chamber data need to be reevaluated. It was also determined that random measurement error can result in skewed flux-estimate errors. Selection of chamber and flux calculation methods should consider the physical characteristics of the soil profile as well as measurement error. The techniques presented here can be used to develop soil- and method-specific error estimates.

Abbreviations: CE, comparative error; CS, crusted surface; DK, disk tillage; DT, deployment time; Exp, exponential model; HM, Hutchinson and Mosier; MB, moldboard plow; NDFE, non-steady-state diffusive flux estimator; NT, no-till; Quad, quadratic model; RE, relative error; TF, temperate forest.

It is widely recognized that non-steady-state chamber methods for estimating soil-to-atmosphere trace gas flux alter concentration gradients at the soil–atmosphere interface due to gas accumulation within chambers during deployment. This effect suppresses the diffusional driving force, resulting in an underestimation of the predeployment flux (Livingston and Hutchinson, 1995; Davidson et al., 2002; Hutchinson and Livingston, 2002). For trace gases that are emitted from soil to atmosphere (e.g., CO_2 and N_2O), systematic underestimation of fluxes has important implications in quantifying greenhouse gas impacts and in accurately determining nutrient budgets. Systematic biases associated with experimental treatments or environmental factors may also confound the interpretation of research data.

Soil physical properties (e.g., bulk density and air-filled porosity) determine the capacity of the soil to store and transport gas, which in turn affects the dynamics of gas accumulation within flux chambers. Soil property effects on chamber trace gas dynamics have been demonstrated theoretically and empirically (Healy et al., 1996; Hutchinson et al., 2000; Conen and Smith, 2000; Butnor et al., 2005). Some studies have attempted to quantify errors in chamber-based flux estimates (reviewed by Davidson et al., 2002). Many studies are limited by the fact that under field conditions no absolute reference for flux is available for comparison with calculated values, although some laboratory experiments have attempted to overcome this problem (Nay et al., 1994). Numerical modeling has also been used to generate theoretical chamber data that can be compared with calculated flux estimates (Hutchinson et al., 2000).

Studies to date have all assumed uniformity of physical properties across the soil profile; however, substantial near-surface gradients in soil physical properties are common. In agricultural soils, tillage operations and vehicle traffic can cause significant variations in bulk density and porosity in the upper 10 to 250 mm (Logsdon and Karlen, 2004; Logsdon and Cambardella, 2000). Surface crusts formed due to erosive forces within the upper 2 to 10 mm can have bulk densities that exceed the underlying soil by 30% or more (Roth, 1997). In forest soils, substantial nonuniformity results from deposition and decomposition of plant residues in surface horizons that are underlain by mineral soils (Gaudinski et al., 2000). And in most soils, vertical gradients in soil water content are commonplace and contribute to variations in air-filled porosity.

There is currently no consensus regarding the most appropriate method for calculating fluxes based on chamber data. Many studies have attempted to minimize errors by adjusting measurement conditions to promote increased linearity in chamber concentration time-series data, while others have

Soil Sci. Soc. Am. J. 72:1410-1417
doi:10.2136/sssaj2008.0019
Received 21 Jan. 2008.
*Corresponding author (rod.venterea@ars.usda.gov).

utilized nonlinear flux calculation methods (Hutchinson and Mosier, 1981; Wagner et al., 1997). Livingston et al. (2006) proposed a theoretical model and recommended using extended chamber deployment times and smaller chamber heights to enhance nonlinearity. The Livingston et al. (2006) model is also based on an assumption of physical uniformity throughout the soil profile. The main objective of the current study was to use a series of numerical simulations to examine how variations in physical characteristics both within and among soil profiles affect gas flux chamber concentrations and influence errors in fluxes estimated using several different calculation schemes.

MATERIALS AND METHODS

Numerical Model Description

Numerical methods were used to solve the diffusion–reaction equation in the form

$$S\frac{\partial C}{\partial t}=\frac{\partial}{\partial z}\left(D_p\frac{\partial C}{\partial z}\right)+\rho P \quad [1]$$

where S is a storage coefficient (m^3 soil air m^{-3} soil), C is the gas-phase trace gas (CO_2 or N_2O) concentration (g C or N m^{-3} gas), t is time (h), D_p is the soil-gas diffusion coefficient (m^3 gas m^{-1} soil h^{-1}), z is soil depth (m), ρ is soil bulk density (g m^{-3}), and P is the soil trace gas production rate (kg C or N kg^{-1} soil h^{-1}). The one-dimensional diffusive transport equation (Eq. [1]) assumes that chamber insertion depth and radius are sufficient to minimize lateral diffusion effects, the chamber is properly vented, and any gas recirculation system is designed to reduce pressure perturbations (Hutchinson and Livingston, 2002; Xu et al., 2006). An important distinction of our application of Eq. [1] in comparison to previous models (Healy et al., 1996; Livingston et al., 2006) is that S, D_p, and ρ were not assumed to be constant throughout z. The storage coefficient was defined as

$$S=\varepsilon+K_H\theta \quad [2]$$

where ε is the volumetric air content (m^3 gas m^{-3} soil), K_H is the Henry's Law partitioning coefficient (m^3 gas m^{-3} H_2O), and θ is the volumetric water content (m^3 H_2O m^{-3} soil). Depending on soil pH, the formation of soluble carbonate species from dissolved CO_2 will also contribute to S and influence chamber gas dynamics (Hutchinson and Rochette, 2003). This can be accounted for by multiplying the final term in Eq. [2] by $\Sigma = 1 + 10^{(pH - pKa)} + 10^{(2pH - pKa - pKb)}$, where K_a ($10^{-6.38}$) and K_b ($10^{-10.38}$) are equilibrium constants for the dissociation of carbonic acid and bicarbonate, respectively (Snoeyink and Jenkins, 1980). To limit the current analysis to soil physical effects, we assumed that $\Sigma = 1$ and confirmed in separate simulations that the CO_2 results were equivalent to assuming pH ≤6.0. The term SC therefore represents total CO_2 or N_2O mass per volume soil contained within the air and liquid phases of the pore space under equilibrium conditions. We also assumed that N_2O production occurred via nitrification under aerobic conditions (Venterea, 2007), with no sink term in Eq. [1]. The primary reason for considering N_2O was to examine the impacts of gas properties on flux-estimate errors.

Soil-gas diffusivity was calculated using the Rolston and Moldrup (2002) model:

$$D_p=D_o\varphi^2\left(\frac{\varepsilon}{\varphi}\right)^{2+3/b} \quad [3]$$

where D_o is the gas diffusivity in free air (m^2 h^{-1}), φ is the total porosity (m^3 m^{-3}), and b is the Campbell pore-size distribution parameter. When the model of Sallam et al. (1984), where $D_p = D_o\varepsilon^{3.1}/\varphi^2$, was used in place of Eq. [3], results were nearly identical. The reported simulations assumed a constant temperature of 20°C and values for K_H of 0.938 and 0.698 m^3 H_2O m^{-3} gas and D_o of 0.0633 and 0.0497 m^2 gas h^{-1} for CO_2 and N_2O, respectively (Wilhelm et al., 1977; Fuller et al., 1966).

Equation [1] was solved by finite-difference techniques described by Venterea and Rolston (2000) using FORTRAN. Temporal discretization was continuously adjusted to maintain numerical mass balance errors <0.01% using time steps ≤30 s and spatial discretization ≤1 mm. Numerical methods were validated by comparing computed fluxes and concentration profiles with steady- and transient-state analytical solutions.

A total soil profile depth (L) of 1 m was assumed with a no-flux boundary condition (BC) imposed at $z = L$. Soil-to-atmosphere gas fluxes were computed from Fick's law with the gradient estimated by the difference in concentration at z = 1 mm and z = 0 using D_p calculated at z = 1 mm.

Simulation Procedure

Each simulation consisted of first assigning vertical distributions of ρ and θ from $z = 0$ to L based on measured data for a variety of soil profile conditions. Distributions of φ and ε were assigned from basic physical relations and S and D_p were then determined from Eq. [2–3]. Vertical distribution of the source term (P) was imposed to generate a specified steady-state CO_2 or N_2O flux. Consistent with the numerical modeling results of Hutchinson et al. (2000) and the analytical solution derived by Livingston et al. (2006), chamber gas concentration dynamics were independent of source vertical distribution. This was confirmed in the current study by comparing the results using differing distributions including exponential decay with depth, Gaussian distributions centered at varying depths, and constant source with depth. After initializing the above distributions, the system was modeled under homogeneous atmospheric conditions (with no flux chamber deployed) by imposing upper BCs of $C(t, 0)$ = 0.17 g C m^{-3} gas or 0.35 mg N m^{-3} gas for CO_2 and N_2O, respectively, and initial conditions of $C(0, z)$ equal to these same values. The simulation was allowed to proceed until a steady-state surface flux (f_o) and vertical soil gas concentration profile were attained. Steady-state conditions were assumed to have been met when (i) the surface flux was within 1% of the theoretical flux calculated from $\int_0^L \rho P dz$ and (ii) the flux and soil gas concentrations did not change by more than 0.001% during a 0.5-d simulation time. Once steady state was reached, chamber deployment was initiated by altering the upper BC at each time step to reflect mass accumulation within a homogeneously mixed chamber. The assumption of well-mixed chamber conditions follows Livingston et al. (2006), who concluded that temperature and pressure gradients within chambers are likely to induce sufficient advection to overwhelm pure diffusive mixing. Surface flux at each time step was used to update the BC at $z = 0$ according to the effective chamber height (h), where h is equivalent to the chamber internal volume divided by its cross-sectional area in contact with the soil. The actual units of h are cubic meters of gas per square meter of soil (or cm^3 gas cm^{-2} soil) but are simplified to meters (or cm). Varying total chamber DTs for each of six h values (5, 10, 15, 20, 25, and 30 cm) at each of three f_o values for CO_2 (36, 90, 180 mg C m^{-2} h^{-1}) and N_2O (0.83, 2.1, and 4.2 mg N m^{-2} h^{-1}) were simulated.

Flux Model Error Analysis

For each simulation, numerical model output of chamber CO_2 or N_2O time vs. concentration was generated and then used to calculate the estimated surface flux (f_{est}) using five different flux models: (i) the non-steady-state diffusive flux estimator (NDFE) model (Livingston et al., 2006), (ii) linear regression, (iii) the nonlinear model of Hutchinson and Mosier (1981) (HM), (iv) a quadratic model (Quad) (Wagner et al., 1997), and (v) an exponential model (Exp). The NDFE estimates were obtained using the nonlinear iterative regression solver described in Livingston et al. (2006) (available at arsagsoftware.ars.usda.gov, verified 17 July 2008) to fit the data to

$$C_c(t)=C_c(0)+\frac{f_{est}\tau}{h}\left[\frac{2}{\sqrt{\pi}}\sqrt{t/\tau}+\exp(t/\tau)\,\mathrm{erfc}\left(\sqrt{t/\tau}\right)-1\right] \qquad [4]$$

where $C_c(t)$ is the chamber CO_2 or N_2O concentration at time t following deployment, $C_c(0)$ is the initial time-zero chamber CO_2 or N_2O concentration, and τ is a regression coefficient. The τ term also has physical meaning for the case of a uniform profile. Simulated $C_c(t)$ data were compiled at 0.15-h intervals using DT values of 1, 2, and 3 h and supplied to the solver. Linear flux model estimates were obtained by linear regression of $C_c(t)$ vs. t with f_{est} calculated from $h(dC_c/dt)$. Deployment times of 0.25, 0.5, and 1 h were analyzed, using output time intervals of 0.0625, 0.125, and 0.333 h, respectively (i.e., five data points per DT including time zero). These same DT values and time intervals were used for the HM, Quad, and Exp models. In the case of the HM flux model, only the initial (t = 0), third, and fifth data point were used, since the model easily accommodates three data points that are equally spaced in time. The Quad model flux estimates were obtained using the LINEST functions in Microsoft Excel (Version 2002) to derive parameters of the quadratic function for $C_c(t)$ and then multiplying the analytical derivative at t = 0 by h. The Exp model flux estimates were obtained using the nonlinear regression solver in Sigma Plot (Version 10.0, Systat Software, San Jose, CA) to fit the data to

$$C_c(t)=C_c(0)+\alpha\left[1-\exp(-\beta t)\right] \qquad [5]$$

where $C_c(0)$, α, and β are regression coefficients and f_{est} is given by $h\alpha\beta$. Equation [5] is similar in form to the model of Nakano et al. (2004).

The estimated predeployment flux (f_{est}) values obtained from each flux model were compared with the steady-state predeployment value achieved by the numerical simulation (f_o). The relative error (RE) of each estimate was calculated as $100(f_{est} - f_o)/f_o$, where a positive RE represents an overestimation of f_o. In addition, the comparative error (CE) is defined as the relative difference in f_{est} for two soil profiles differing in physical properties but having the same f_o. The CE_i was calculated as $100(RE_i - RE_{ref})/(RE_{ref} + 100)$, where RE_{ref} is the relative error for the reference profile and RE_i is the relative error for profile i. A positive CE_i value represents an overestimation of flux from profile i as a percentage of the estimated flux from the reference profile. All comparisons were made using the moldboard plow (MB) profile (see below) as the reference. Effects of chamber trace gas concentration measurement precision on the resulting errors were evaluated by assuming that measurement error was normally distributed with a mean of 0 and standard deviations (σ) of 0, 1.0, or 2.5%. The σ values are hereafter referred to as "measurement error." Chamber trace gas concentration time series generated by the numerical model were subjected to 1000 Monte Carlo simulations using the RiskAMP add-in for Microsoft Excel or algorithms incorporated into the NDFE solver (similar results were obtained with both methods) before analysis by each flux model.

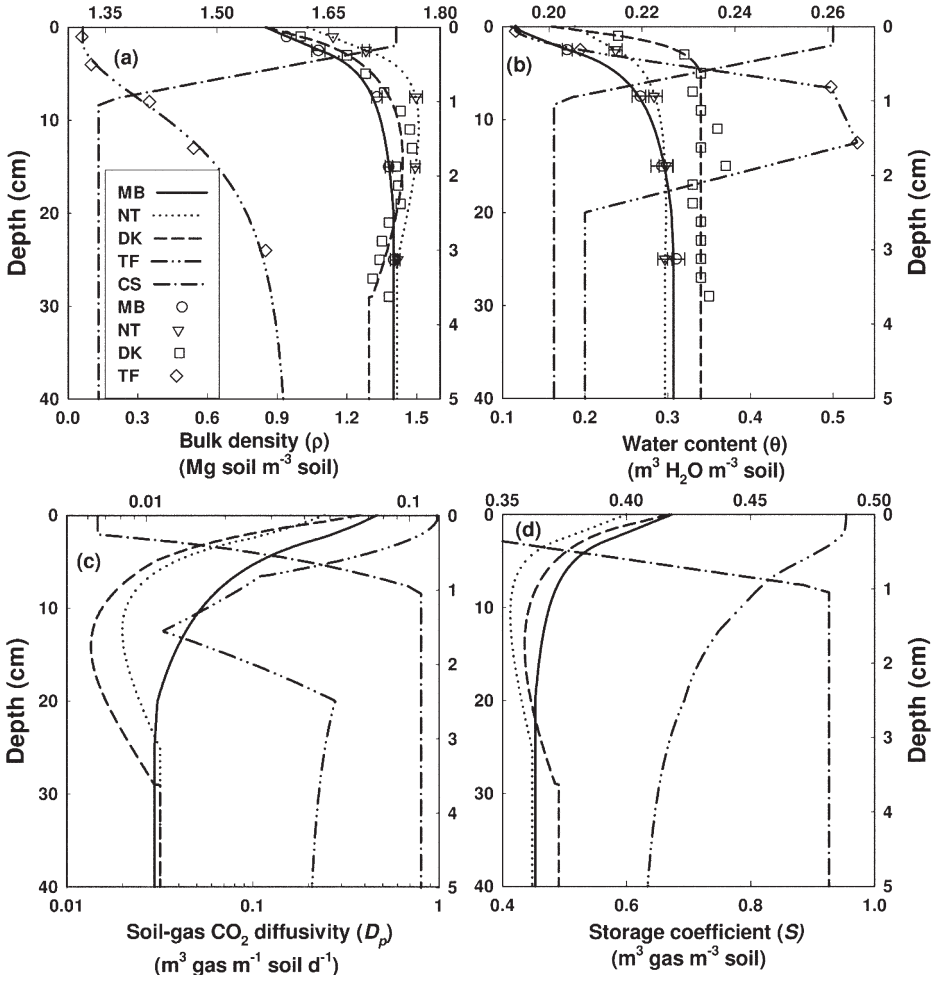

Fig. 1. Vertical distributions of (a) bulk density, (b) volumetric water content, (c) soil-gas CO_2 diffusivity, and (d) storage coefficient for CO_2 in moldboard plow (MB), no-till (NT), disk tillage (DK), temperate forest (TF), and crusted surface (CS) soil profiles. In (a and b), symbols are measured data used to generate regression functions (lines) that were used as inputs to the numerical model (no data shown for CS profile). In (c and d), values were calculated using Eq. [2–3]. The right-hand vertical and upper horizontal axes in each graph have different scales and apply to the CS profile only.

Soil Profiles

Five different soil profiles, each displaying vertical variation in ρ and θ, were used as inputs to the numerical model (Fig. 1a and 1b): (i) the MB pro-

file used data from a Waukegan silt loam (fine-silty over sandy or sandy-skeletal, mixed, superactive, mesic Typic Hapludoll) in southeastern Minnesota under conventional moldboard plow tillage and corn (*Zea mays* L.)–soybean [*Glycine max* (L.) Merr.] management for 15 yr, sampled August 2006 (Venterea and Stanenas, 2008); (ii) the no-till (NT) profile used data from the same soil, field, and date as the MB profile except under no-till management for 15 yr; (iii) the disk tillage (DK) profile used mean data from three fields in central Iowa with soils ranging in texture from loam to clay loam under disk tillage and corn–soybean management sampled April 1995 (Logsdon and Cambardella, 2000); (iv) the temperate forest (TF) profile used data from a Canton fine sandy loam (coarse-loamy over sandy or sandy-skeletal, mixed, semiactive, mesic Typic Dystrudept) in a hardwood forest in central Massachusetts, with bulk density and soil C data taken from Gaudinski et al. (2006) and water content data for the upper 15 cm taken from Venterea et al. (2004), assuming that θ decreased with depth below 15 cm (Davidson et al., 2006); and (v) the crusted surface (CS) profile was a hypothetical profile based on data in Roth (1997). The CS profile was constructed using the mean ρ for the upper 40 cm of the MB profile except in the upper 1 cm, where bulk density data for a surface-crusted silt loam from Roth (1997) were used. These data showed a nearly linear increase in bulk density in the upper 1 cm to ~0.4 Mg m^{-3} above the undisturbed soil value. The ρ profile used for CS is also similar to experimental and modeled soil crusts examined by Bresson et al. (2004) and others. A uniform gravimetric water content of 0.15 kg H_2O kg^{-1} soil was assumed for the CS profile. For the other profiles, measured data were fit to regression equations to generate continuous functions for ρ and θ that were used as numerical model inputs (Fig. 1a and 1b). For all profiles except TF, a particle density (ρ_s) of 2.65 Mg m^{-3} was assumed. For TF, ρ_s varied as a function of organic matter content as described by Davidson et al. (2006). For profiles MB, NT, DK, and CS, a value for *b* of 9.6 in Eq. [3] was used based on soil-water retention data for the Minnesota Waukegan silt loam (Spaans and Baker, 1996). For TF, a *b* value of 2.81 was used (Davidson et al., 2006; Savage and Davidson 2001). For all the nonuniform profiles except CS, corresponding uniform profiles were also examined, with each assumed to have constant ρ, ρ_s, and θ corresponding to the mean values in the upper 40 cm of the corresponding nonuniform profile, except for θ in the uniform TF profile, which we assumed was 0.3 m^3 H_2O m^{-3} soil (Table 1).

Table 1. Bulk density (ρ), water content (θ), storage coefficients (*S*), and soil-gas diffusivities (D_p) in uniform profiles and derived quantity λ in uniform and corresponding nonuniform profiles.

Profile†	ρ	θ	Gas	*S*	D_p	λ = $(SD_p)^{-1}$		
						Calculated‡	By regression§	Nonuniform range‡¶
	Mg m^{-3}	m^3 m^{-3}		m^3 m^{-3}	m^3 m^{-1} d^{-1}	d m^{-2}#		
MB	1.34	0.28	CO_2	0.48	0.054	38.91	38.79	3.2–72.5
			N_2O	0.41	0.042	57.74	57.59	4.2–113
NT	1.43	0.29	CO_2	0.44	0.034	65.83	65.65	6.8–120
			N_2O	0.38	0.027	99.35	98.58	9.4–187
DK	1.33	0.33	CO_2	0.48	0.029	73.25	73.03	4.0–170
			N_2O	0.40	0.023	112.26	111.02	4.9–190
TF	0.74	0.30	CO_2	0.67	0.132	11.2	11.0	1.1–40
			N_2O	0.60	0.123	13.5	13.4	1.4–62

† MB, moldboard plow; NT, no-till; DK, disk tillage; TF, temperate forest.

‡ Calculated directly from *S* and D_p values using Eq. [7].

§ Calculated using Eq. [7] and τ values obtained by the non-steady-state diffusive flux estimator solver.

¶ Range of values across full depth of corresponding nonuniform profile. Range for nonuniform crusted surface profile = 19–470 d m^{-2}.

Actual units of λ are d m^4 soil m^{-6} gas.

RESULTS AND DISCUSSION

Chamber Gas Dynamics

Simulated chamber CO_2 concentrations following 3 h of chamber deployment are shown in Fig. 2. Chamber concentrations diverged from one another within approximately 0.25 and 0.5 h for *h* = 5 and 25 cm, respectively, except for the nonuniform NT and DK profiles, which exhibited nearly identical time series. Greater divergence was shown with the nonuniform profiles and

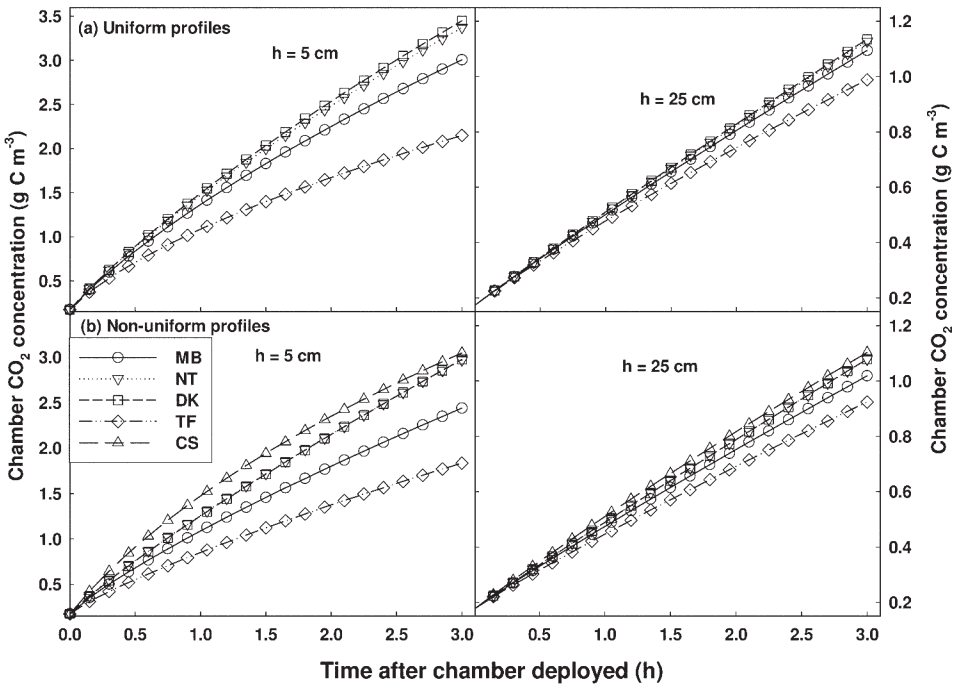

Fig. 2. Simulated chamber CO_2 concentrations vs. time after the chamber was deployed in (a) uniform and (b) nonuniform moldboard plow (MB), no-till (NT), disk tillage (DK), temperate forest (TF), and crusted surface (CS, nonuniform only) profiles for a predeployment flux of 90 mg C m^{-2} h^{-1} and effective chamber heights (*h*) of 5 and 25 cm.

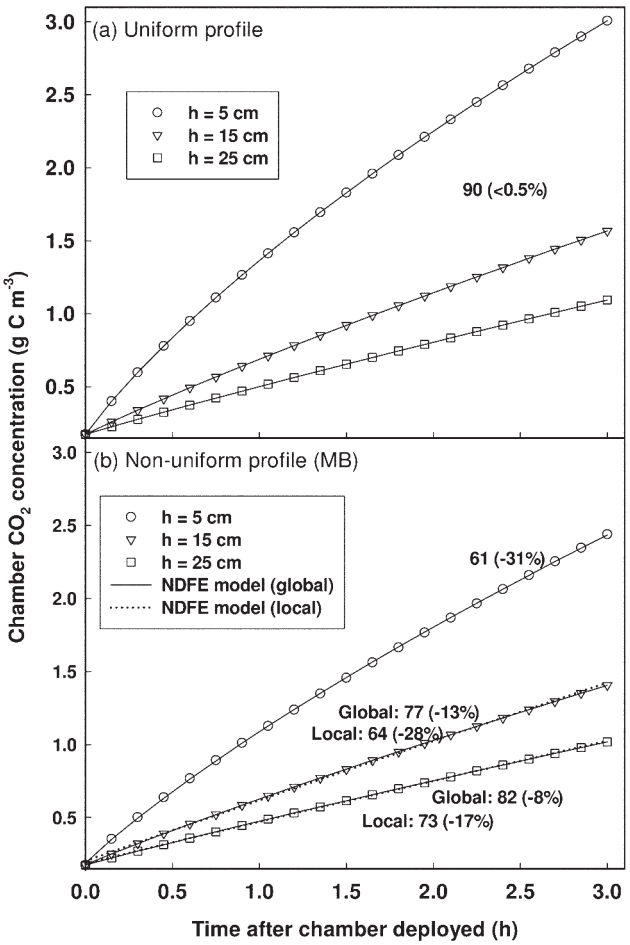

Fig. 3. Simulated chamber CO_2 concentration vs. time after the chamber was deployed for (a) the moldboard plow (MB) uniform profile, and (b) the MB nonuniform profile for a predeployment flux of 90 mg C m^{-2} h^{-1} and varying effective chamber heights (*h*). Symbols are numerical model output. Lines represent Eq. [4] with parameters obtained by the non-steady-state diffusive flux estimator (NDFE) regression solver. Dotted lines (which overlap solid lines) for *h* = 15 and 25 in (b) use parameter sets obtained from convergence of the solver to local minima in sums of squares. Values are fluxes estimated by the NDFE model and corresponding relative errors.

with the lower *h* value. These trends in chamber gas dynamics are the result of differences among profiles in the proportion of total gas produced within the soil that was emitted into the chamber vs. that which accumulated in the soil following chamber deployment. Profiles with lower ρ and higher ε values (and correspondingly higher D_p and *S* values) in the upper 5 cm (TF and MB) exhibited the least increases in chamber trace gas concentration (Fig. 2) while accumulating proportionately more gas within the soil. Conversely, the least porous profiles (NT and CS) exhibited the greatest increases in chamber gas and accumulated proportionately less gas within the soil. For example, the numerical results showed that the nonuniform TF profile accumulated CO_2 within the soil equivalent to 70 and 31% of the total CO_2 produced during the 3-h deployment for *h* = 5 and 25 cm, respectively, compared with 48 and 15% for the nonuniform NT profile. There are two important aspects of these chamber gas dynamics with respect to flux-estimate errors: (i) the divergence of concentration data from linearity, which results in an underestimation of predeployment flux using the simple regression model $f_{est} = h(dC_c/dt)$, and (ii) the divergence of concentration data for different profiles from one another, which implies that errors in flux estimation may vary among soil profiles.

Flux Model Error Analysis

The NDFE model potentially eliminates flux-estimate errors because, in theory, it accounts for soil physical properties based on a solution to the diffusion equation analogous to Eq. [1] albeit with the additional assumptions that *S* and D_p are both constant in *z*. For theoretically uniform profiles, Livingston et al. (2006) showed that the dynamics illustrated in Fig. 2 can be described exactly by Eq. [4] with

$$\tau = \frac{h^2}{SD_p} \qquad [6]$$

This was confirmed by the current numerical simulations. When numerical output using uniform profiles was supplied to the NDFE solver, the parameter sets obtained produced nearly identical agreement between Eq. [4] and the numerical output. This is first illustrated in Fig. 3a for the uniform MB profile for *h* = 5, 15, and 25 cm. Conversely, when values of *h*, *S*, D_p, and f_o that were used as inputs to the numerical model were entered directly into Eq. [4], identical agreement between the output data and Eq. [4] were also shown. We also evaluated the term

$$\lambda \equiv \frac{\tau}{h^2} = \left(SD_p\right)^{-1} \qquad [7]$$

where λ is an inherent soil characteristic that is independent of the chamber height and therefore is constant for a uniform soil profile. For the uniform profiles, λ values derived from the τ values obtained by the NDFE solver agreed with the λ values calculated directly from *S* and D_p values (Table 1), which is additional confirmation of agreement between Eq. [4] and the numerical model for uniform profiles.

While flux-estimate errors generated by the NDFE model were <0.5% when applied to uniform profiles (Fig. 3a), more substantial errors were found with the nonuniform profiles. This is first illustrated in Fig. 3b for the MB nonuniform profile, where RE values of –31, –13, and –8% were found for *h* values of 5, 15, and 25 cm, respectively. Thus, the NDFE model diverges substantially from the numerical solutions, and the divergence increases with decreasing *h*. Another important aspect of the NDFE model is shown in Fig. 3b, i.e., the possible convergence to multiple parameter sets due to the existence of local and global minima in residuals sums of squares (SS). While this was pointed out by Livingston et al. (2006), the results shown in Fig. 3b highlight the importance of careful monitoring of residuals when using the NDFE model. Locally converged parameter sets can result in agreement between the model and chamber data that is nearly indistinguishable (at least visually) from globally converged parameter sets. In the error analysis below, we selected the "best" solutions based on minimizing SS.

For all of the nonuniform profiles examined, the NDFE estimate error increased with decreasing *h* and with increasing DT, while errors for the uniform profiles were close to zero and relatively insensitive to *h* and DT (Fig. 4). Relative error values generated by the NDFE model at each *h* and DT value for

the nonuniform profiles were nearly identical using predeployment fluxes of 36, 90, or 180 mg C m^{-2} h^{-1} (data not shown), and were slightly less pronounced for N_2O than for CO_2 for a given h and DT (Fig. 4). The errors shown here for the nonuniform soils demonstrate that the analytical solution given by Eq. [4] under the assumption of constant S and D_p diverges from numerical solutions to Eq. [1] given varying distributions of S and D_p shown in Fig. 1. In other words, while the quantity λ calculated in Eq. [7] is assumed in Eq. [4] to be constant, actual λ values range widely across depth in the nonuniform profiles, as shown in Table 1.

Unlike the NDFE model, the other flux models generated substantial errors in the uniform profiles (Fig. 5). For the nonuniform profiles, RE values for the linear and HM models displayed the same trends with h and DT as the NDFE model. The Quad and Exp models performed nearly identically to the HM model across all conditions and therefore their results are not shown. For a DT value of 1 h, errors from the NDFE model were generally less pronounced compared with other models. The one exception was the CS profile, where the NDFE model overestimated f_o to a greater extent (RE = 17% at h = 5 cm, Fig. 4) than the HM model underestimated f_o (RE = –6% at h = 5 cm, Fig. 5). Like the NDFE model, errors for all flux models were invariant with f_o and slightly less pronounced for N_2O than CO_2. For any given model, there was substantial variation in RE values between profiles, resulting in CE values that also increased with decreasing h (Fig. 6).

The effects of soil-gas diffusivity and storage in regulating chamber gas dynamics are expressed mathematically by Eq. [4] and [6]. The physical basis for these effects was explained by Hutchinson et al. (2000). Soils having lower D_p and S (and therefore greater λ) require steeper vertical gradients in gas concentration to achieve the same steady-state f_o and have less storage capacity compared with profiles with higher D_p and S. Thus, when a chamber is deployed over a soil with higher λ, a greater proportion of gas produced during deployment is transmitted to the chamber and less accumulates in the soil compared with a profile with lower λ.

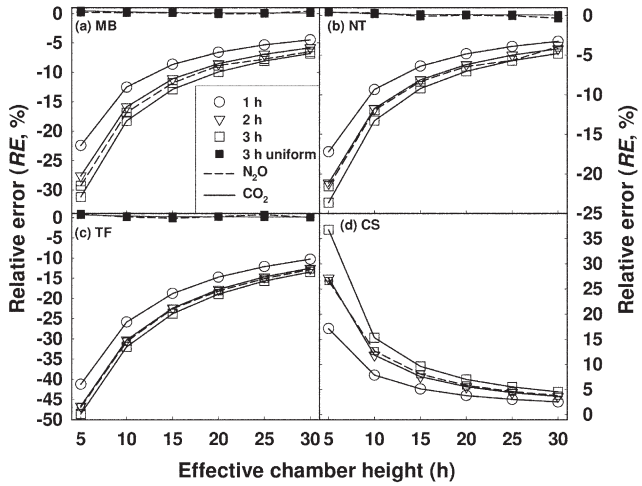

Fig. 4. Relative errors in flux of CO_2 (solid lines) and N_2O (dashed lines) estimated by the non-steady-state diffusive flux estimator (NDFE) model for nonuniform (open symbols) and uniform (closed symbols) (a) moldboard plow (MB), (b) no-till (NT), (c) temperate forest (TF), and (d) crusted surface (CS) profiles at varying effective chamber heights and chamber deployment times. Note different vertical axis scales.

Measurement Error and Other Factors

The above results assume that chamber gas concentrations supplied to the flux models were determined with 100% accuracy. The effects of measurement error (σ) on RE values for each model under specific conditions are shown in Fig. 7. Flux models varied considerably in their response to varying σ for the case of h = 25 cm and DT = 0.25 h (Fig. 7a). The linear and NDFE models were most stable, while the HM model (which used data from only three of seven samples) was least stable. These results also indicate that normally distributed measurement error can be translated into skewed flux-estimate errors. While the nonlinear models (HM, Quad, and Exp) produced nearly identical mean RE values, the HM and Exp models showed increasingly positive skewness (mean > median) as σ increased. DT values >0.25 h are often required for logis-

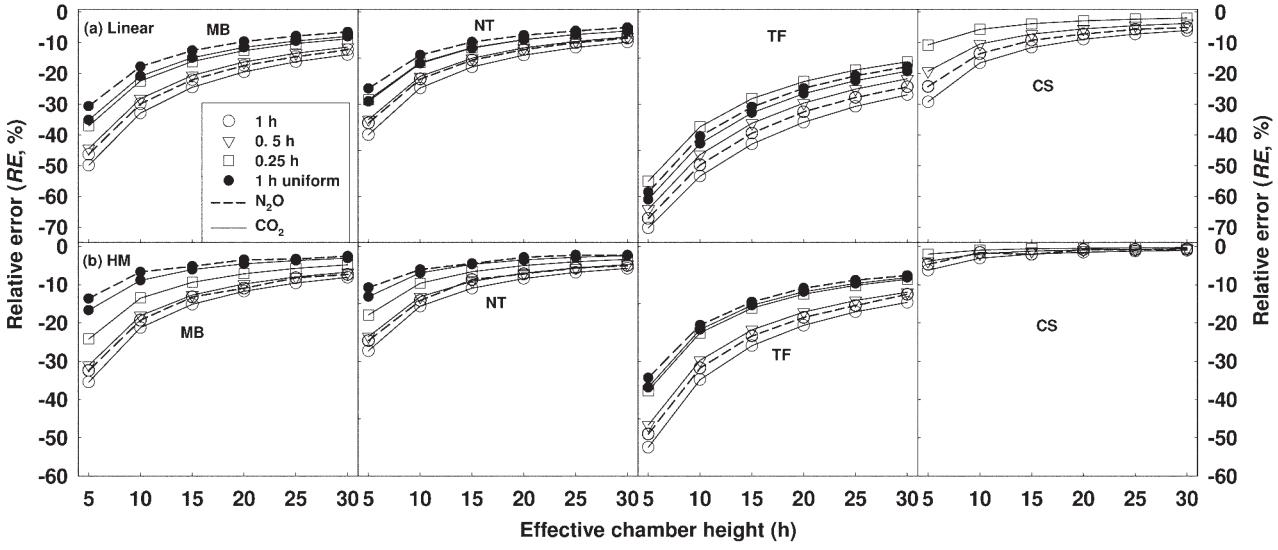

Fig. 5. Relative errors in flux of CO_2 (solid lines) and N_2O (dashed lines) estimated by (a) linear and (b) Hutchinson and Mosier (HM) models for nonuniform (open symbols) and uniform (closed symbols) moldboard plow (MB), no-till (NT), temperate forest (TF), and crusted surface (CS, nonuniform only) profiles at varying effective chamber heights and chamber deployment times of 0.25, 0.5, and 1 h.

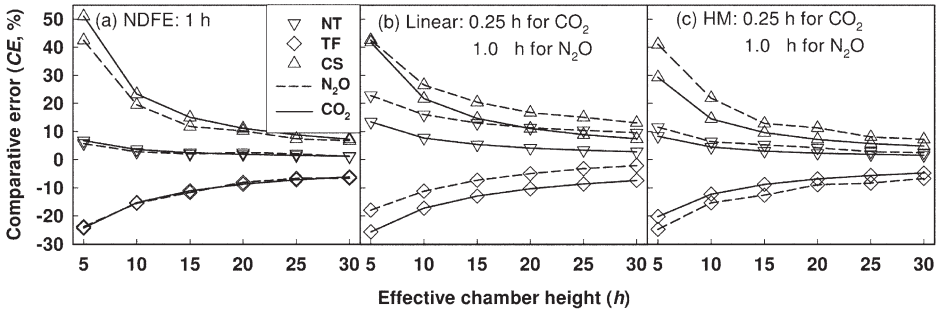

Fig. 6. Comparative errors for fluxes of CO_2 (solid lines) and N_2O (dashed lines) at varying effective chamber heights estimated by (a) the non-steady-state diffusive flux estimator (NDFE) model with 1-h deployment time, and (b) the linear and (c) the Hutchinson and Mosier (HM) models with 0.25- and 1-h deployment times for CO_2 and N_2O, respectively, in nonuniform no-till (NT), temperate forest (TF), and crusted surface (CS) profiles using the moldboard plow (MB) profile as reference.

tical reasons, i.e., when multiple chamber replicates are being sampled manually and when portable, fast-response gas analyzers are not readily available. Researchers commonly use DT values ranging from 0.5 to 1 h for measuring N_2O flux, with three to five samples collected during deployment (e.g., McLain and Martens, 2006; Amos et al., 2005). Figure 7b illustrates how RE can be decreased by decreasing the DT from 1.2 to 0.6 h. The nonlinear models provided increased accuracy, but with the trade-off of decreased precision compared with the linear model. The number of samples collected had little effect.

We also examined the response of the NDFE model regression solver to the units of gas concentration used. When units of grams of C per cubic meter or milligrams of N per cubic meter were used with t units of hours and h units of centimeters, the solver was inefficient at converging to global minima. When concentration values were increased by a factor of 10 for CO_2 (equivalent to using units of dg C m^{-3}) or 1000 for N_2O (g N m^{-3}), the solutions converged more efficiently to global minima. These effects were presumably due to numerical factors and the selection of initial parameter estimates. These findings again point out the need for careful interpretation when using regression analysis that can converge to multiple solutions. Knowledge of the expected τ values based on soil properties could be useful in eliminating suboptimal solutions. In the current case, we had knowledge of the "correct" τ and f_o generated by the numerical model. In practice, however, this is problematic in nonuniform soils since τ may range across more than an order of magnitude throughout the profile (Table 1).

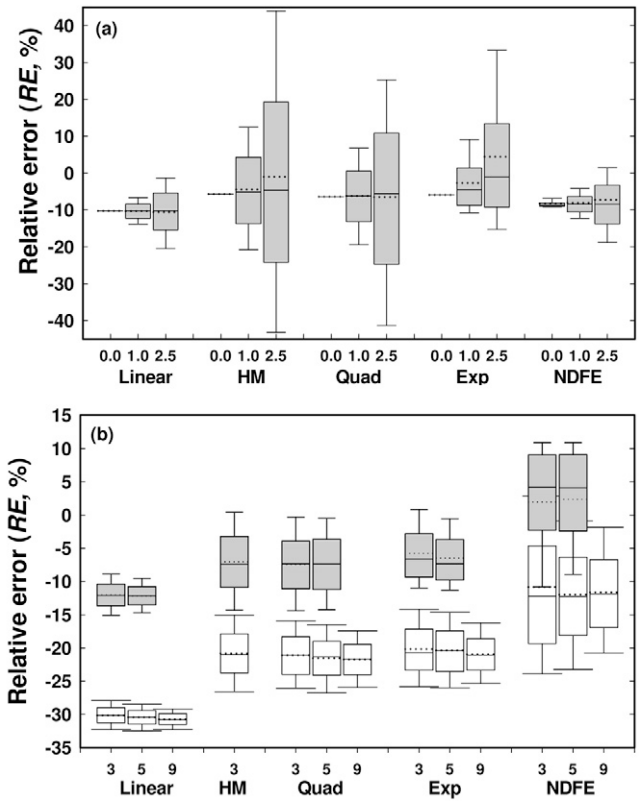

Fig. 7. Box plots showing the effects of (a) measurement error (σ), and (b) deployment time (DT) and number of samples, on relative error (RE) values of fluxes estimated by linear, Hutchinson and Mosier (HM), quadratic (Quad), exponential (Exp), and non-steady-state diffusive flux estimator (NDFE) models in the moldboard plow profile. In (a), RE values are for CO_2 fluxes obtained with chamber height h = 25 cm and seven samples collected during a DT of 0.25 h with σ values of 0, 1.0, or 2.5%. In (b), RE values are for N_2O fluxes obtained with h = 25 cm using three, five, or nine samples collected during a DT of 1.2 h (open boxes) or 0.6 h (shaded boxes) assuming σ = 2.5%. Each box summarizes 1000 Monte Carlo simulations where solid vertical lines in each box represent 10th, 25th, 50th, 75th, and 90th percentiles, and dotted lines, where visible, are means.

Practical Recommendations

To determine the flux-estimate error for a completely uniform profile, measured values of total and air-filled porosity and pH (for CO_2) can first be used to calculate τ from Eq. [2], [3], and [6], allowing theoretical data to be generated from Eq. [4] for a given h, DT, $C_c(0)$, and f_o (e.g., Fig. 2a). The RE can then be determined for a given sampling protocol and flux calculation scheme (excluding the NDFE model) by selecting the appropriate points from the time series and subjecting them to the scheme. Because of the invariance of RE to f_o, the error analysis will be applicable to all f_o. In nonuniform soil this procedure cannot be used in a straightforward way, however, because λ and τ are likely to vary across a wide range throughout the profile. Since Eq. [1] does not lend itself to analytical solutions for nonconstant D_p and S, numerical techniques are the only option for highly accurate error analysis in nonuniform soil. A conservative approach would be to determine the lower limit of λ within the profile by measurement or estimation, and then proceed as described above for the uniform case. This analysis would provide the maximum RE for that profile, which may be useful in establishing protocols to minimize error and in interpreting data; however, this approach is likely to greatly overestimate the actual RE. A more accurate analysis can be done using spatially resolved measurements of soil profile characteristics in conjunction with the approach used in this study (the numerical model is available on request). It is also recommended that measurement error be considered in

this analysis, since we show here that nonlinear models can result in skewed and highly variable estimates.

CONCLUSIONS

For all models, flux-estimate errors in nonuniform soils were minimized with larger effective h and shorter DTs. Thus, the suggestion by Livingston et al. (2006) to minimize h and extend DT to enhance nonlinearity when using the NDFE model needs to be reconsidered, unless the soil under study can be assumed to be physically uniform. The recommendations presented here can be used to estimate errors for a given set of soil conditions, protocols, and calculation schemes. The recommendation that maximizing h will minimize error needs to be taken with caution, since this assumes a homogeneous chamber atmosphere. The validity of this assumption is likely to fail as h increases above some limit in the absence of induced mixing. Further studies are needed to define these limits. Additional work is also needed to examine the effects of nonsteady soil conditions and soil consumption processes (e.g., of N_2O during denitrification) on errors in chamber-based flux estimates, which to our knowledge have not been addressed in previous studies.

ACKNOWLEDGMENTS

This work was assisted by discussions with Feike Dijkstra and Kurt Spokas, and was supported by the USDA Agricultural Research Service under the ARS GRACEnet Project.

REFERENCES

Amos, B., T.J. Arkebauer, and J.W. Doran. 2005. Soil surface fluxes of greenhouse gases in an irrigated maize-based agroecosystem. Soil Sci. Soc. Am. J. 69:387–395.

Bresson, L.M., C.J. Moran, and S. Assouline. 2004. Use of bulk density profiles from x-radiography to examine structural crust models. Soil Sci. Soc. Am. J. 68:1169–1176.

Butnor, J.R., K.H. Johnsen, and C.A. Maier. 2005. Soil properties influence estimates of soil CO_2 efflux from three chamber-based measurement systems. Biogeochemistry 73:283–301.

Conen, F., and K.A. Smith. 2000. An explanation of linear increases in gas concentration under closed chambers used to measure gas exchange between soil and the atmosphere. Eur. J. Soil Sci. 51:111–117.

Davidson, E.A., K.E. Savage, S.E. Trumbore, and W. Borken. 2006. Vertical partitioning of CO_2 production within a temperate forest soil. Global Change Biol. 12:944–956.

Davidson, E.A., K. Savage, L.V. Verchot, and R. Navarro. 2002. Minimizing artifacts and biases in chamber-based measurements of soil respiration. Agric. For. Meteorol. 113:21–37.

Fuller, E.N., P.D. Schettler, and J.C. Giddings. 1966. A new method for prediction of binary gas-phase diffusion coefficients. Ind. Eng. Chem. 58:19–27.

Gaudinski, J.B., S.E. Trumbore, E.A. Davidson, and S. Zheng. 2000. Soil carbon cycling in a temperate forest: Radiocarbon-based estimates of residence times, sequestration rates and partitioning of fluxes. Biogeochemistry 51:33–69.

Healy, R.W., R.G. Striegl, T.F. Russell, G.L. Hutchinson, and G.P. Livingston. 1996. Numerical evaluation of static-chamber measurements of soil–atmosphere gas exchange: Identification of physical processes. Soil Sci. Soc. Am. J. 60:740–747.

Hutchinson, G.L., and G.P. Livingston. 2002. Soil-atmosphere gas exchange. p. 1159–1182. *In* J.H. Dane and G.C. Topp (ed.) Methods of soil analysis. Part 4. SSSA Book Ser. 5. SSSA, Madison, WI.

Hutchinson, G.L., G.P. Livingston, R.W. Healy, and R.G. Striegl. 2000. Chamber measurement of surface–atmosphere trace gas exchange: Numerical evaluation of dependence on soil, interfacial layer, and source/sink properties. J. Geophys. Res. Atmos. 105:8865–8875.

Hutchinson, G.L., and A.R. Mosier. 1981. Improved soil cover method for field measurement of nitrous oxide fluxes. Soil Sci. Soc. Am. J. 45:311–316.

Hutchinson, G.L., and P. Rochette. 2003. Non-flow-through steady-state chambers for measuring soil respiration: Numerical evaluation of their performance. Soil Sci. Soc. Am. J. 67:166–180.

Livingston, G.P., and G.L. Hutchinson. 1995. Enclosure-based measurement of trace gas exchange: Applications and sources of error. p. 164–205. *In* P.A. Matson and R.C. Harriss (ed.) Biogenic trace complexes. 2nd ed. Spec. Publ. 17. Blackwell Sci. Ltd., Oxford, UK.

Livingston, G.P., G.L. Hutchinson, and K. Spartalian. 2006. Trace gas emission in chambers: A non-steady-state diffusion model. Soil Sci. Soc. Am. J. 70:1459–1469.

Logsdon, S.D., and C.A. Cambardella. 2000. Temporal changes in small depth-incremental soil bulk density. Soil Sci. Soc. Am. J. 64:710–714.

Logsdon, S.D., and D.K. Karlen. 2004. Bulk density as a soil quality indicator during conversion to no-tillage. Soil Tillage Res. 78:143–149.

McLain, J., and D.A. Martens. 2006. Moisture controls on trace gas fluxes in semiarid riparian soils. Soil Sci. Soc. Am. J. 70:367–377.

Nakano, T., T. Sawamoto, T. Morishita, G. Inoue, and R. Hatano. 2004. A comparison of regression methods for estimating soil–atmosphere diffusion gas fluxes by a closed-chamber technique. Soil Biol. Biochem. 36:107–113.

Nay, M.S., K.G. Mattson, and B.T. Bormann. 1994. Biases of chamber methods for measuring soil CO_2 efflux demonstrated with a laboratory apparatus. Ecology 75:2460–2463.

Rolston, D.E., and P. Moldrup. 2002. Gas diffusivity. p. 1113–1139. *In* J.H. Dane and G.C. Topp (ed.) Methods of soil analysis. Part 4. SSSA Book Ser. 5. SSSA, Madison, WI.

Roth, C.H. 1997. Bulk density of surface crusts: Depth functions and relationships to texture. Catena 29:223–237.

Sallam, A., W.A. Jury, and J. Letey. 1984. Measurement of gas diffusion coefficient under relatively low air-filled porosity. Soil Sci. Soc. Am. J. 48:3–6.

Savage, K.E., and E.A. Davidson. 2001. Interannual variation of soil respiration in two New England forests. Global Biogeochem. Cycles 15:337–350.

Snoeyink, V.L., and D. Jenkins. 1980. Water chemistry. John Wiley & Sons, New York.

Spaans, E.J., and J.M. Baker. 1996. The soil freezing characteristic: Its measurement and similarity to the soil moisture characteristic. Soil Sci. Soc. Am. J. 60:13–19.

Venterea, R.T. 2007. Nitrite-driven nitrous oxide production under aerobic soil conditions: Kinetics and biochemical controls. Global Change Biol. 13:1798–1809.

Venterea, R.T., P.M. Groffman, L. Verchot, A. Magill, and J. Aber. 2004. Gross nitrogen process rates in temperate forest soils exhibiting symptoms of nitrogen saturation. For. Ecol. Manage. 196:129–142.

Venterea, R.T., and D.E. Rolston. 2000. Mechanistic modeling of nitrite accumulation and nitrogen oxide gas emissions during nitrification. J. Environ. Qual. 29:1741–1751.

Venterea, R.T., and A.J. Stanenas. 2008. Profile analysis and modeling of reduced tillage effects on soil nitrous oxide flux. J. Environ. Qual. 37:1360–1367.

Wagner, S.W., D.C. Reicosky, and R.S. Alessi. 1997. Regression models for calculating gas fluxes measured with a closed chamber. Agron. J. 89:279–284.

Wilhelm, E., R. Battino, and R.J. Wilcock. 1977. Low-pressure solubility of gases in water. Chem. Rev. 77:219–262.

Xu, L., M.D. Furtaw, R.A. Madsen, R.L. Garcia, D.J. Anderson, and D.K. McDermitt. 2006. On maintaining pressure equilibrium between a soil CO_2 flux chamber and the ambient air. J. Geophys. Res. Atm. 111(D08S10), doi:10.1029/2005JD006435.